Supporting Information

Leveraging Donor-Acceptor Mutual Dilution to Finely Tune Vertical Phase Separation for High-Performance Semitransparent Organic Solar Cells

Guohao Qin [a], Xinyuan Ren [a], Shiyong You [a], Lei Tang [a], Yaqi Pei [a], Lifu Zhang [b], Longbin Li [c], Bending Zhang [b], Han Young Woo [d], Hyeong Hui Kim [d], Feiyan Wu*[a], Jiabin Liu*[a], and Lie Chen*[a]

[a] College of Chemistry and Chemical Engineering/Film Energy Chemistry for Jiangxi Provincial Key Laboratory (FEC), Nanchang University, Nanchang 330031, PR China.

[b] Key Laboratory of Fluorine and Silicon for Energy Materials and Chemistry of Ministry of Education, Jiangxi Normal University, 99 Ziyang Avenue, Nanchang 330022, China.

[c] College of Chemistry and Materials Science, Gannan Normal University, Ganzhou 341000, China.

[d] Department of Chemistry College of Science, Korea University 145 Anam-ro, Seongbuk-gu, Seoul 02841, Republic of Korea.

*Corresponding Author

E-mail addresses: feiywu@ncu.edu.cn (F. Wu), liujiabin@ncu.edu.cn (J. Liu), chenlie@ncu.edu.cn (L. Chen).

Experimental Section

Materials:

PCE10-2F was synthesized in our previous work, Y6 was purchased from Derthon Optoelectronic Materials Science Technology Co LTD (Shenzhen, China).

Measurements

Optical characterizations:

UV-vis absorption spectra were recorded on an Agilent series UV-Vis-NIR spectrophotometer. All film samples were spin-cast on quartz slice substrates. The photoluminescence spectra (PL) were measured by photoluminescence spectroscopy (Hitachi F-7000).

Electrochemical characterizations:

Cyclic voltammetry (CV) was performed by a Zahner IM6e electrochemical workstation, using Ag/AgCl as the reference electrode, a Pt plate as the counter electrode, and a glassy carbon as the working electrode. Polymers were drop-cast onto the electrode from chloroform solutions to form thin films. 0.1 mol L^{-1} tetrabutylammonium hexafluorophosphate in anhydrous acetonitrile was used as the supporting electrolyte. The scan rate was 0.05 V s^{-1}. The E_{HOMO} and E_{LUMO} are calculated as referring to formulas (1) and (2).

$$E_{HOMO} = -(Eox+4.4)\ eV \quad (1)$$

$$E_{LUMO} = -(Ered+4.4)\ eV \quad (2)$$

AFM characterizations:

The specimen for AFM measurements was prepared using the same procedures for fabricating devices, but without PNDIT-F3N /Ag on top of the active layer.

GIWAXS measurements:

The GIWAXS measurement was carried out at the PLS-II 6A U-SAXS beamline of the Pohang Accelerator Laboratory in Korea. The X-rays coming from the in-vacuum undulator (IVU) were monochromated (wavelength l = 1.10994 Å) using a double

crystal monochromator and focused both horizontally and vertically (450 (H) x 60 (V) um^2 in FWHM @ the sample position) using K-B type mirrors. The grazing incidence wide-angle X-ray scattering (GIWAXS) sample stage was equipped with a 7-axis motorized stage for the fine alignment of the sample, and the incidence angles of the X-ray beam were set to be 0.12°-0.16° for the neat and blend films. The GIWAXS patterns were recorded with a 2D CCD detector (Rayonix SX165) and an X-ray irradiation time of 100 s, dependent on the saturation level of the detector.

Depth-dependent light absorption spectroscopy:

Depth-related light absorption spectra by using low-pressure oxygen plasma to incrementally etch the active film, which is monitored by a light absorption spectrometer. Including these sublayer absorption spectra into the transfer matrix optical model yields depth-dependent optical properties and exciton generation profiles. The exciton generation rate (G) was estimated by formula (3-4):

$$Q_{act}(\chi,\lambda) = \frac{1}{2} c\varepsilon_0 \alpha n |E(\chi,\lambda)|^2 \quad (3)$$

$$G(x) = \int_{\lambda_{begin}}^{\lambda_{end}} \frac{\lambda}{hc} Q_{act}(\chi,\lambda) d\lambda \quad (4)$$

Where Q_{act} is energy dissipation, α and n represent the absorption coefficient and refractive index of the active layer respectively, $|E(\chi,\lambda)|^2$ is modulus squared of the optical electric field. λ is the test wavelength, λ_{begin} and λ_{end} are transmission through the ITO and absorption onset of the active layer.

Electron and Hole mobility measurements:

Hole and electron mobilities were measured using the space charge limited current (SCLC) method, with hole-only device of ITO/PEDOT:PSS/active layer/MoO_3/Ag for hole mobility measurement and the electron-only devices used a diode configuration of ITO/ZnO/active layer/ PNDIT-F3N /Ag by taking the current-voltage curve in the range of -5~5 V. The SCLC mobilities were calculated by the MOTT-Gurney equation, which is described by:

$$J = 9\varepsilon_0\varepsilon_r uV^2/8L^3 \quad (5)$$

where J is the current density, L is the film thickness of active layer, ε_0 is the permittivity of free space (8.85×10^{-12} F m^{-1}), ε_r is the relative dielectric constant of the transport medium, u is the hole or electron mobility, V is the internal voltage in the device and $V = V_{appl}-V_r-V_{bi}$, where V_{appl} is the applied voltage to the device, V_r is the voltage drop due to contact resistance and series resistance across the electrodes, and V_{bi} is the built-in voltage due to the relative work function difference of the two electrodes

Electrochemical Impedance Spectroscopy (EIS):

EIS was conducted using a Hioki LCR Meter. The measurements were performed using conditions that had an applied bias of open-circuit voltage of OSC in the dark, and a frequency ranging from 3 MHz to 200 Hz. The recombination resistance (R_{rec}) can be calculated from formula (5):

$$R_{rec} = \left(\frac{1}{R_{bm}} + \frac{1}{R_{mm}} + \frac{1}{R_{sf}}\right)^{-1} \quad (6)$$

where R_{bm} is the recombination rate of bimolecular recombination, otherwise known as band-to-band recombination, R_{mm} is the recombination rate of monomolecular recombination, otherwise known as bulk trap-assisted recombination or Shockley–Read–Hall recombination, and where Rsf is the recombination rate of surface trap-assisted recombination.

Detailed V_{loss} measurements:

Highly Sensitive EQE was measured by using an integrated system (PECT-600, Enlitech), where the photocurrent was amplified and modulated by a lock-in instrument. The FTPS spectra were calibrated by a germanium detector. Electroluminescence (EL) quantum efficiency (EQE_{EL}) measurements were performed by applying external voltage/current sources through the devices (REPS, Enlitech). EQE_{EL} measurements were carried out from 0 to 3 V. Details of optical Egap determination. The EQE is interpreted as a superposition of distribution of step functions with a step at Egap having a certain probability distribution. This probability distribution can be obtained from the derivative dEQE/dE. The part where the probability is greater than half of the maximum

is integrated to get an average bandgap.

Calculation of AVT:

The AVT is calculated using

$$AVT = \frac{\int T(\lambda)V(\lambda)S(\lambda)d(\lambda)}{\int P(\lambda)S(\lambda)d(\lambda)} \quad (7)$$

where λ is the wavelength, *T* is the transmission, *V* is the normalized photopic spectral response of the eye, and S is the solar photon flux (AM1.5G). It is estimated by taking the average of the transparency of the devices in the visible region (380–740 nm) based on the photonic response of the human eye.

Temperature-dependent UV-vis absorption spectra:

Considering that the absorption peaks of the polymer donor PCE10-2F and the small molecule acceptor Y6 partially overlap in the range of approximately 700-750 nm. Therefore, we separately conduct temperature-dependent UV-vis absorption spectra on M-PCE10-2F (PCE10-2F: Y6 = 0.95: 0.05, 10mg/ml) and pure 0.05Y6 (0.5mg/ml). Then, we subtracted the absorption spectrum of pure 0.05Y6 from the absorption spectrum of M-PCE10-2F at each temperature point to obtain the corrected absorption spectrum of S-PCE10-2F, which completely excludes the absorption contribution of Y6 in the overlapping region.

Device fabrication

Opaque device fabrication:

The device is fabricated with ITO/PEDOT:PSS/active layer/ PNDIT-F3N /Ag traditional structure. The ITO coated glass substrates were cleaned by ultrasound for 15 minutes in sequence in water/detergent, water, acetone and isopropanol, and then treated in ultraviolet-ozone for 1400 seconds. The PEDOT:PSS solution was spin-coated on top of the cleaned ITO-coated glass substrate and the PEDOT:PSS film thickness was approximately 25 nm. After annealing at 150 °C for 20 min, the substrates were transferred into a glove box. For the solar cells based on a SD operating condition, PCE10-2F with a concentration of 8 mg mL^{-1} in CF were spun onto the

PEDOT: PSS layers at 2200 rpm for 40s form the front layer, Y6 with a concentration of 10 mg mL^{-1} in CF, and DIB of 10 mg mL^{-1} was added, then spun onto the PCE10-2F layers at 2000 rpm for 40s. After annealing at 100 °C for 10 min. The PNDIT-F3N was dissolved in methanol at 1mg mL^{-1} and spin-coated on the active layer at 3000 rpm for 30s. Finally, 90-nanometer thick Ag layers were deposited on the active layer under high vacuum of ~3×10^{-4}Pa. The overlapping area of the cathode and anode was 4 square millimeters. *J-V* curves of devicesbased on polymer donor: Y6 were measured under the standard AM 1.5G spectrum of 100 MW cm^{-2}.

Semitransparent device fabrication

The device is fabricated with ITO/PEDOT:PSS/active layer/ PNDIT-F3N/Ag traditional structure. The ITO coated glass substrates were cleaned by ultrasound for 15 minutes in sequence in water/detergent, water, acetone and isopropanol, and then treated in ultraviolet-ozone for 1400 seconds. The PEDOT:PSS solution was spin-coated on top of the cleaned ITO-coated glass substrate and the PEDOT:PSS film thickness was approximately 25 nm. After annealing at 150°C for 20 min, then the substrates were transferred into a glove box. PCE10-2F with a concentration of 8 mg mL^{-1} in CF was spun onto the PEDOT: PSS layers at 2200 rpm for 40s from the front layer, Y6 with a concentration of 10 mg mL^{-1} in CF, and DIB of 10 mg mL^{-1} was added, then spun onto the PCE10-2F layers at 2000 rpm for 40s. After annealing at 100 °C for 10 min. The PNDIT-F3N was dissolved in methanol at 1mg mL^{-1} and spin-coated on the active layer at 3000 rpm for 30s. Finally, 15nm or 25nm thickness Ag and layers were deposited on the active layer under high vacuum of ~3×10^{-4}Pa. Then, MoO_3 (35 nm) was evaporated onto the surface of Ag. The overlapping area of the cathode and the anode was 4 square millimeters. *J-V* curves of ST-OSC devices were measured under the standard AM 1.5G spectrum of 100 MW cm^{-2}.

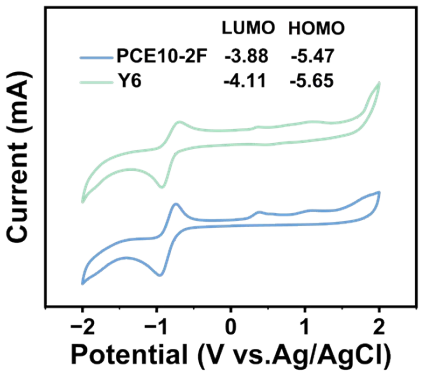

Figure S1. The cyclic voltammogram and Energy level of PCE10-2F and Y6.

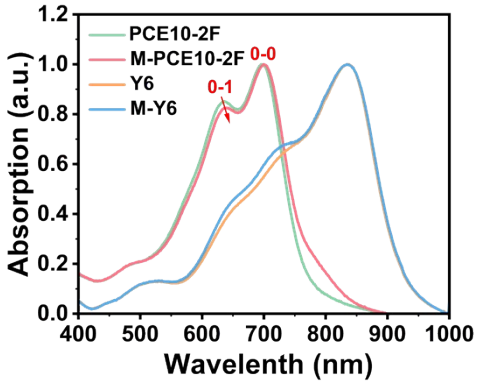

Figure S2. Normalized UV-vis absorption spectra of PCE10-2F, Y6, M-PCE10-2F and M-Y6 films.

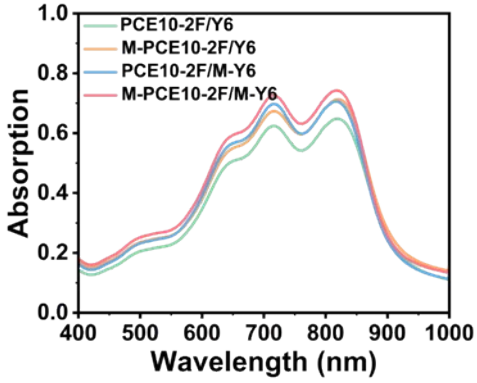

Figure S3. UV-vis absorption spectra of blend films.

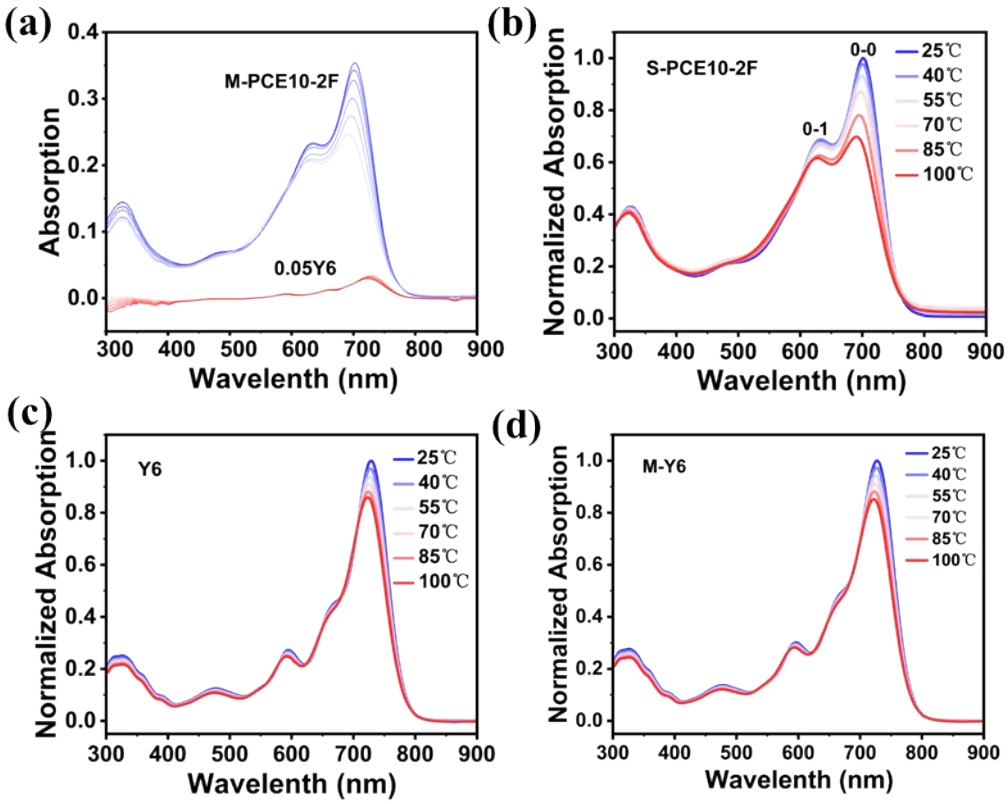

Figure S4. Temperature-dependent UV-vis absorption spectra of the M-PCE10-2F ,0.05Y6, S-PCE10-2F, Y6, and M-Y6 solutions in the temperature range of 25-100℃.

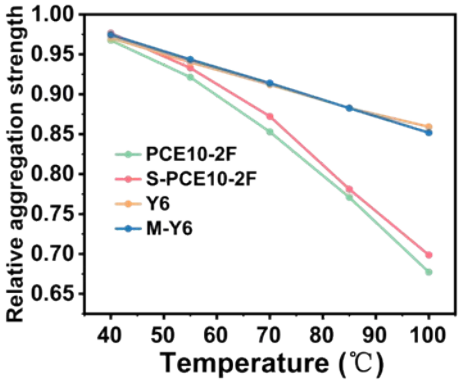

Figure S5. Plot of relative aggregation strength versus solution temperature.

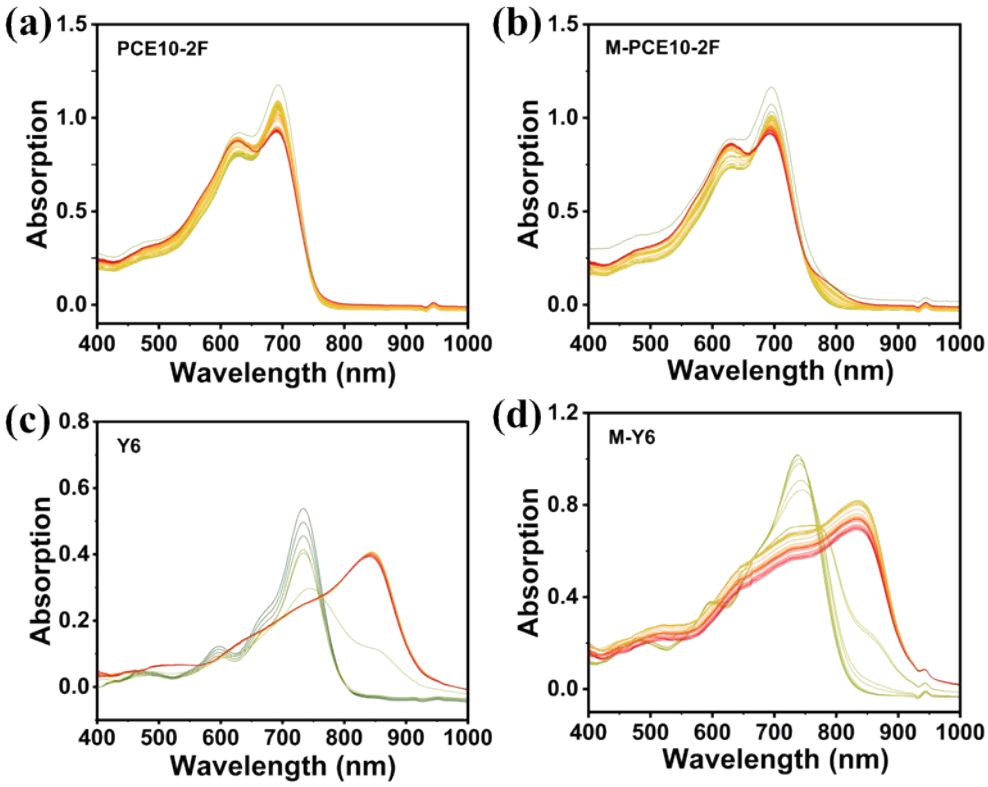

Figure S6. The absorption spectra at representative time points for a) PCE10-2F, b) M-PCE10-2F, c) Y6 and d) M-Y6.

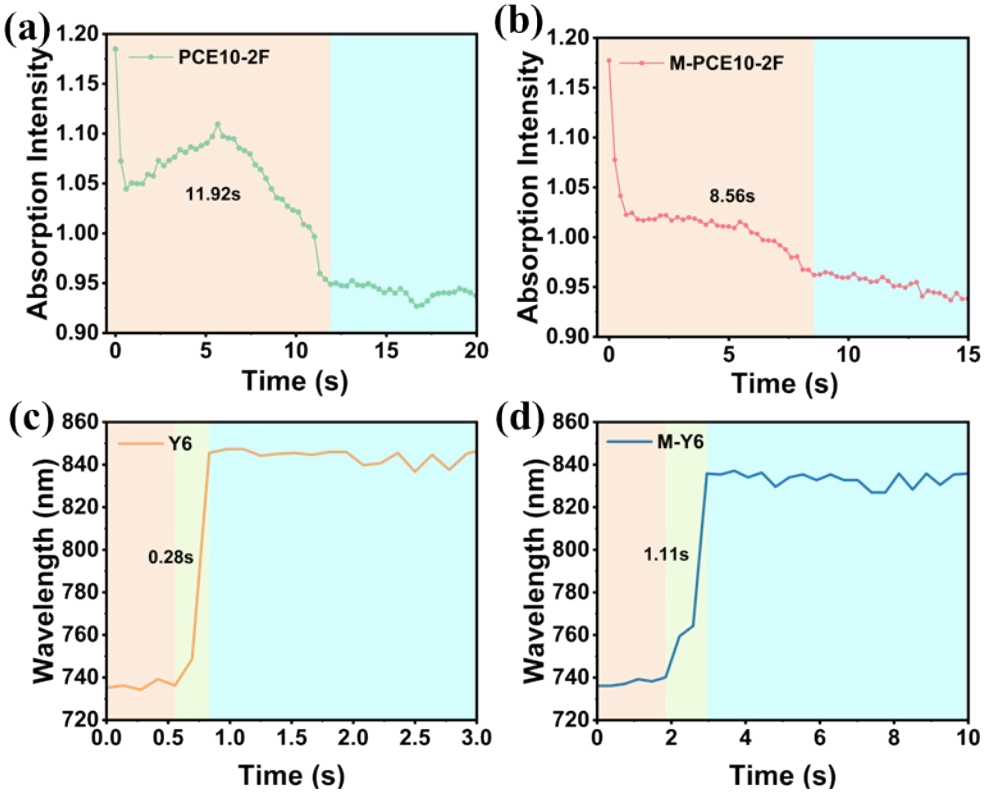

Figure S7. The time of film formation of the donor layer and evolution of the acceptor

layer peak position in-situ UV-vis absorption spectra.

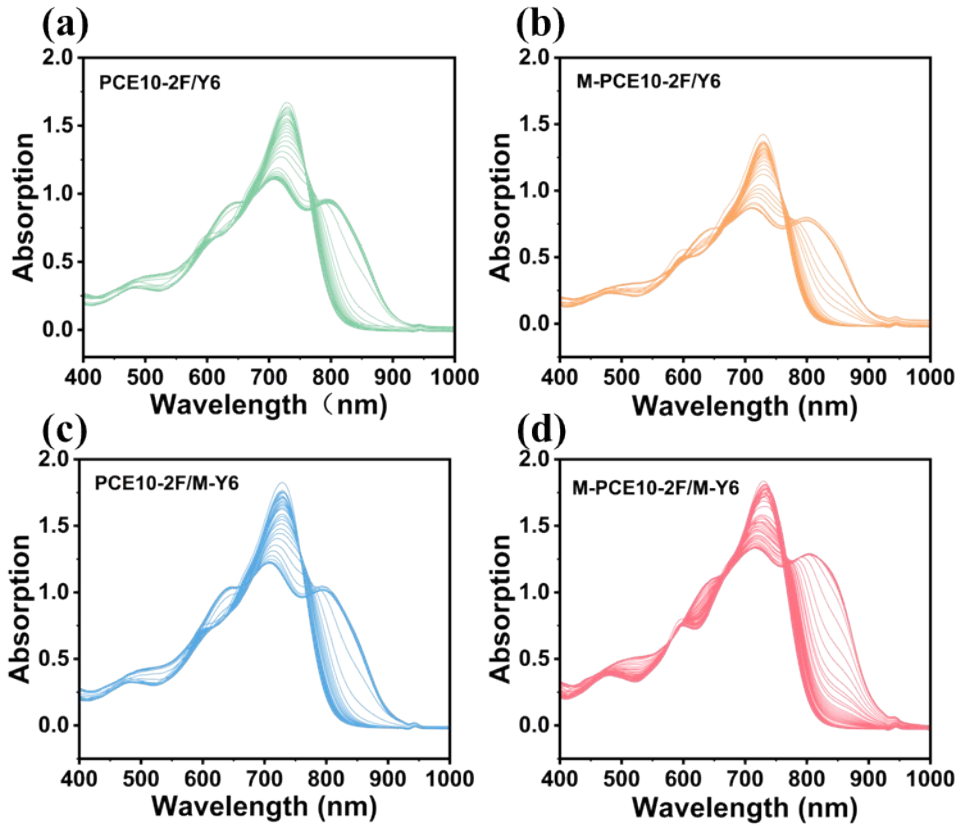

Figure S8. The absorption spectra at representative time points for a) PCE10-2F/Y6, b) M-PCE10-2F/Y6, c) PCE10-2F/M-Y6 and d) M-PCE10-2F/M-Y6.

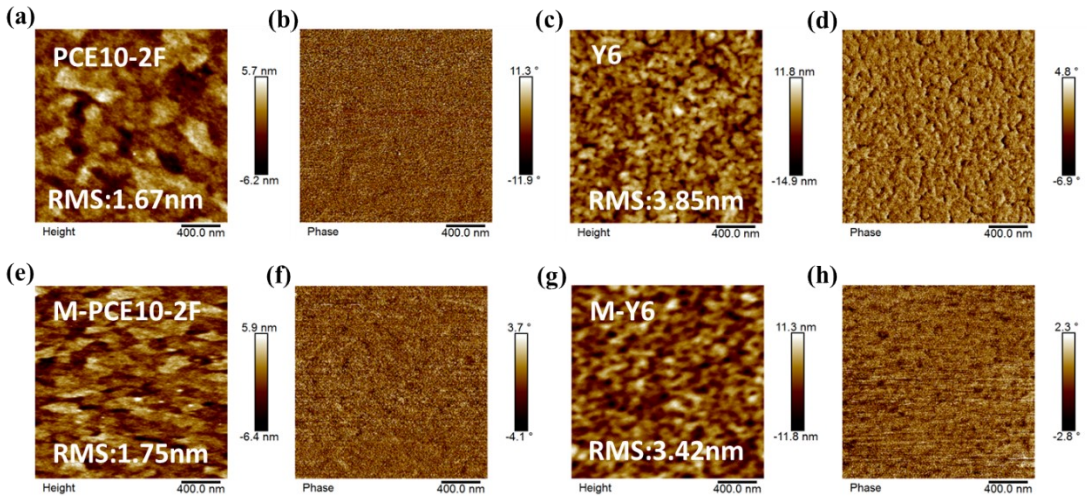

Figure S9. AFM height images and phase images of a, b) PCE10-2F, c, d)Y6, e, f) M-PCE10-2F, g, h) M-Y6.

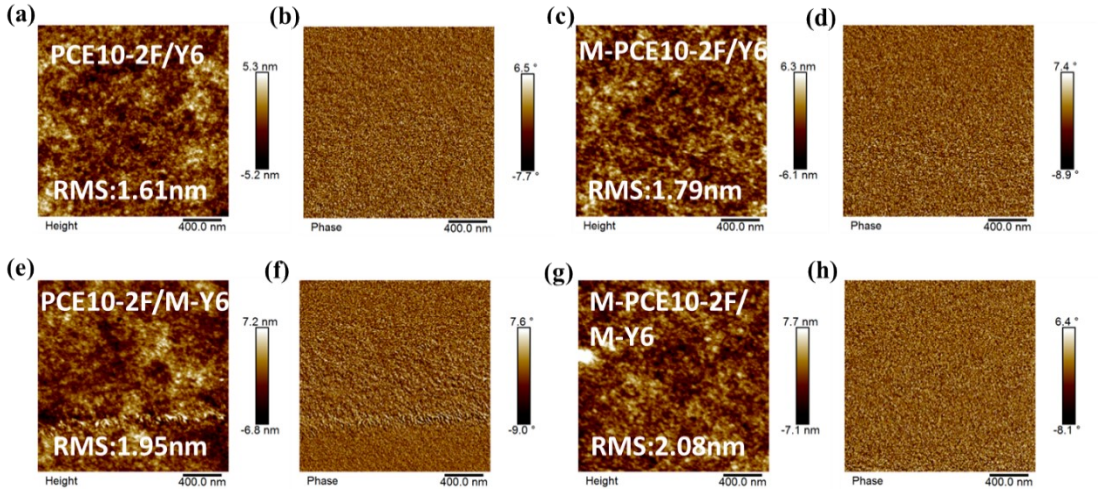

Figure S10. AFM height images and phase images of a, b) PCE10-2F/Y6, c, d) M-PCE10-2F/Y6, e, f) PCE10-2F/M-Y6, g, h) M-PCE10-2F/M-Y6.

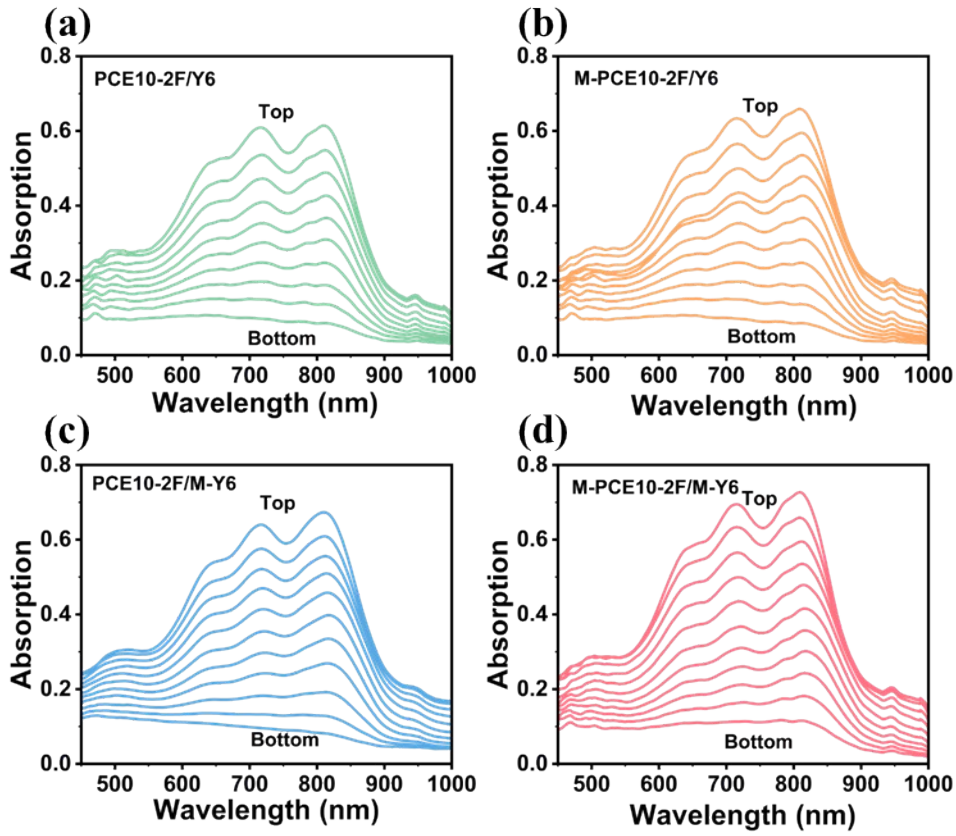

Figure S11. Film-depth-dependent absorption spectroscopy of a) PCE10-2F/Y6, b)M-PCE10-2F/Y6, c) PCE10-2F/M-Y6 and d) M-PCE10-2F/M-Y6 films.

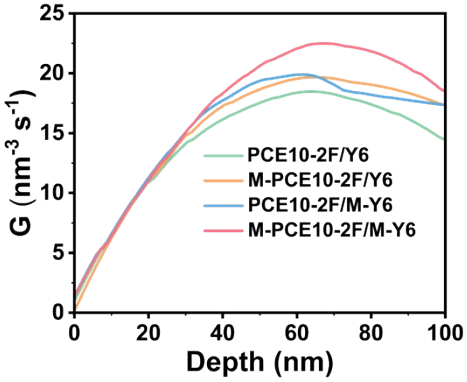

Figure S12. The dependence of the simulated exciton generation rate (G) of PCE10-2F/Y6, M-PCE10-2F/Y6, PCE10-2F/M-Y6 and M-PCE10-2F/M-Y6 films.

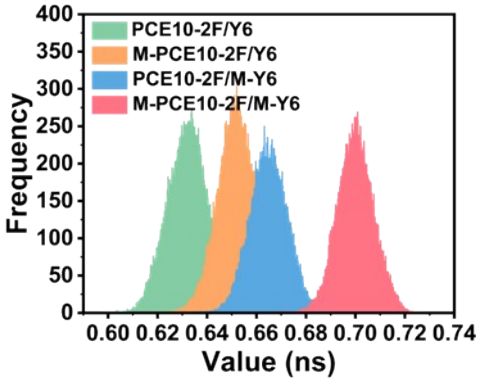

Figure S13. Fluorescence lifetime normal distribution chart of PCE10-2F/Y6, M-PCE10-2F/Y6, PCE10-2F/M-Y6 and M-PCE10-2F/M-Y6 films.

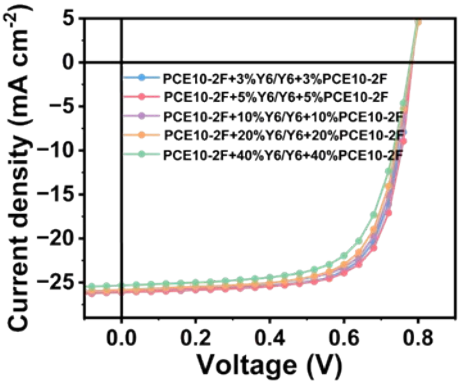

Figure S14. *J-V* characteristic curves based on M-PCE10-2F/M-Y6 systems with different mass fractions.

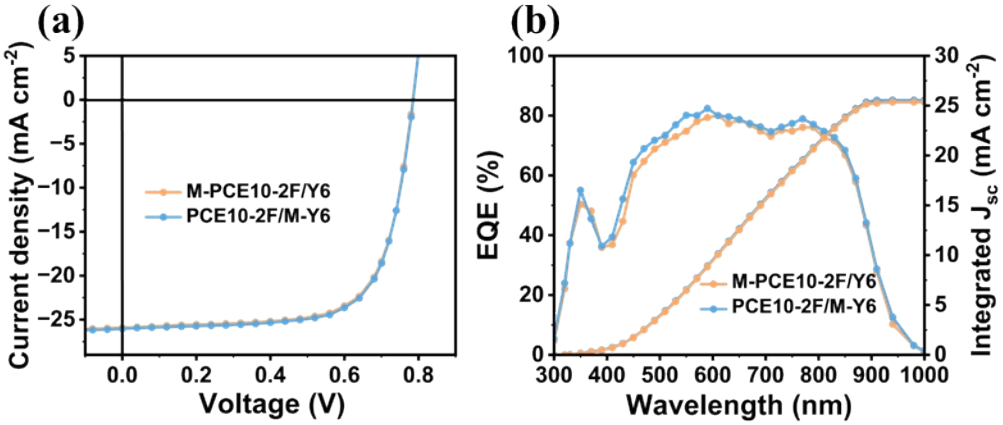

Figure S15. a) *J-V* characteristic curves of M-PCE10-2F/Y6 and PCE10-2F/M-Y6. b) EQE curves of M-PCE10-2F/Y6 and PCE10-2F/M-Y6.

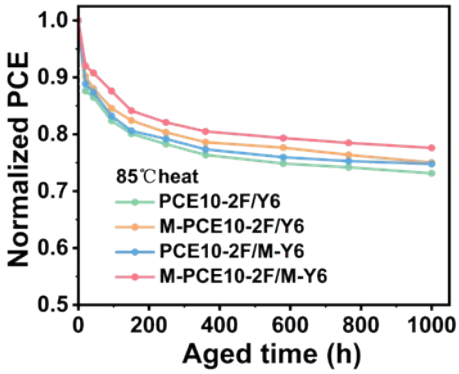

Figure S16. The PCE decay curves under 85 °C continuously annealing in N_2-filled glovebox based on PCE10-2F/Y6, M-PCE10-2F/Y6, PCE10-2F/M-Y6 and M-PCE10-2F/M-Y6 devices.

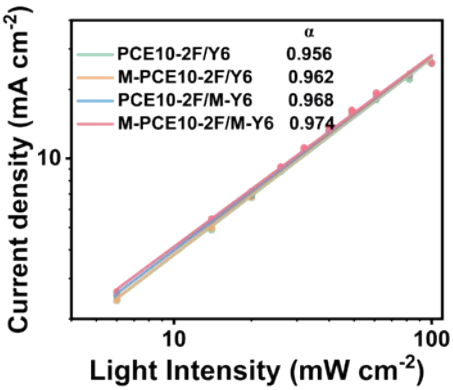

Figure S17. Dependence of J_{sc} on light intensity.

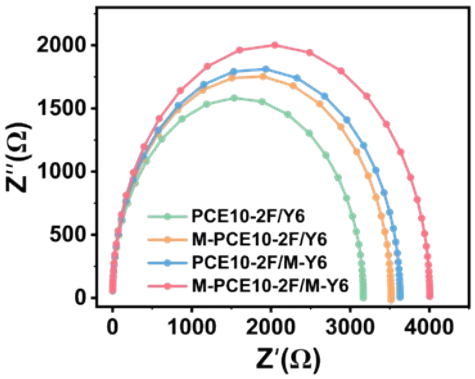

Figure S18. Nyquist plot of P-BHJ, T-BHJ and P-PHJ devices under the dark condition at *V*oc bias (Equivalent electrical circuit model with consideration of interfacial resistance and recombination resistance employed for EIS fitting of the OSCs). The single semicycle in the Nyquist plot is fitted by an equivalent circuit, which includes the interfacial resistance (R_{int}) at the surfaces of the active layer and the recombination resistance (R_{rec}) inside the active layer.

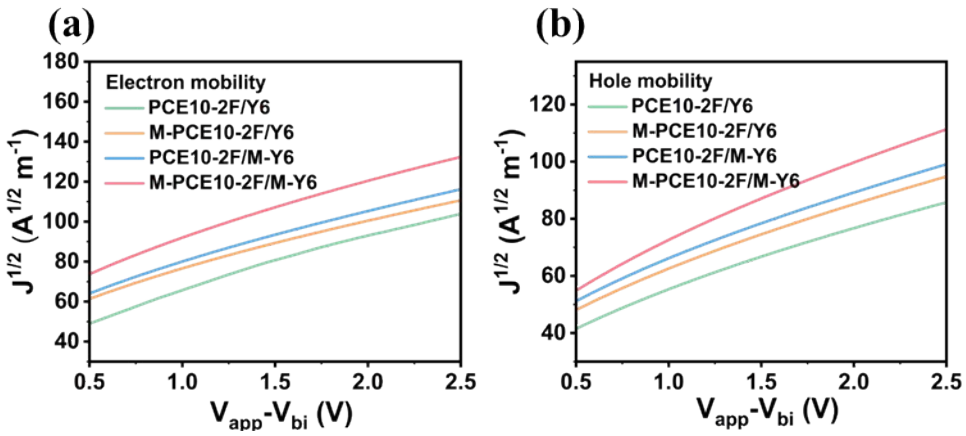

Figure S19. Electron and hole mobility for a, b) PCE10-2F/Y6, M-PCE10-2F/Y6, PCE10-2F/M-Y6 and M-PCE10-2F/M-Y6.

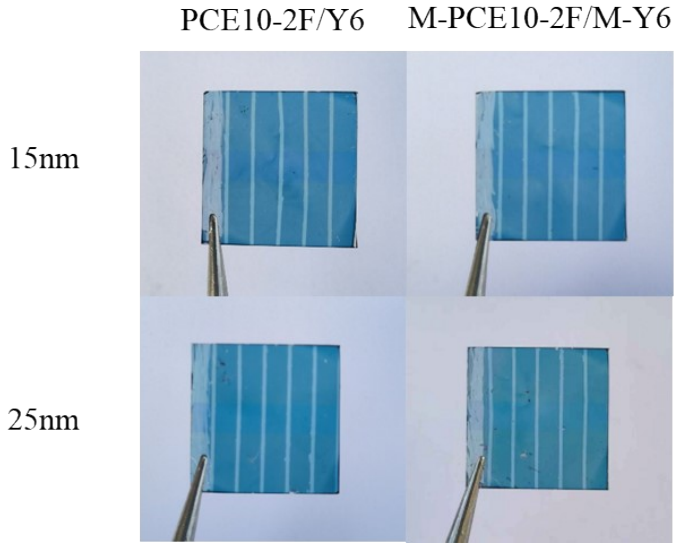

Figure S20. The images of the semitransparent devices PCE10-2F/Y6 and M-PCE10-2F/M-Y6 under 15 nm and 25 nm silver conditions.

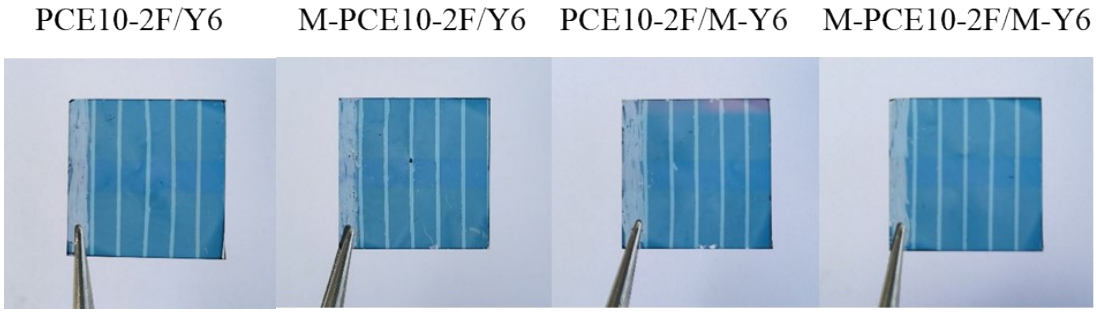

Figure S21. The images of the semitransparent devices PCE10-2F/Y6, M-PCE10-2F/Y6, PCE10-2F/M-Y6, and M-PCE10-2F/M-Y6 under 15 nm silver conditions.

Table S1. The ratio of $I_{0\text{-}0}$ of PCE10-2F, Y6, S-PCE10-2F, and M-Y6 solutions at different temperatures.

	I_{40}/I_{25}	I_{55}/I_{25}	I_{70}/I_{25}	I_{85}/I_{25}	I_{100}/I_{25}
PCE10-2F	0.967	0.921	0.853	0.771	0.677
S-PCE10-2F	0.977	0.933	0.872	0.781	0.699
Y6	0.971	0.940	0.912	0.883	0.859
M-Y6	0.975	0.944	0.914	0.883	0.852

Table S2. Detailed GIWAXS information of the peak for neat films.

	Out-of-plane				In plane			
	π-π stacking cell axis (010)				unit cell long axis (100)			
	q (Å^{-1})	*d*-spacing (Å)	FWHM (Å^{-1})	CCL (Å)	*q* (Å^{-1})	*d*-spacing (Å)	FWHM (Å^{-1})	CCL (Å)
PCE10-2F	1.598	3.932	0.387	16.24	0.264	23.800	0.119	52.73
M-PCE10-2F	1.623	3.871	0.373	16.84	0.263	23.890	0.121	51.99
Y6	1.707	3.681	0.240	26.13	0.282	22.281	0.129	48.82
M-Y6	1.717	3.659	0.299	21.05	0.283	22.202	0.142	44.36

Table S3. Detailed GIWAXS information of the peak for the blend films.

	Out-of-plane				In plane			
	π-π stacking cell axis (010)				unit cell long axis (100)			
	q (Å^{-1})	*d*-spacing (Å)	FWHM (Å^{-1})	CCL (Å)	*q* (Å^{-1})	*d*-spacing (Å)	FWHM (Å^{-1})	CCL (Å)
PCE10-2F/Y6	1.687	3.724	0.344	18.28	0.277	22.68	0.159	39.52
M-PCE10-2F/Y6	1.693	3.711	0.338	18.61	0.278	22.601	0.166	37.84
PCE10-2F/M-Y6	1.699	3.698	0.336	18.70	0.276	22.765	0.164	38.37
M-PCE10-2F/M-Y6	1.698	3.700	0.326	19.26	0.280	22.440	0.175	35.88

Table S4. The photovoltaic parameters of OSCs based on M-PCE10-2F/M-Y6 system with different mass fractions.

Active layer	V_{OC} (V)	J_{SC} (mA/cm^2)	FF (%)	PCE (%)
PCE10-2F+3%Y6/Y6+3%PCE10-2F	0.786	26.05	70.72	14.51
PCE10-2F+5%Y6/Y6+5%PCE10-2F	**0.790**	**26.25**	**72.08**	**14.98**
PCE10-2F+10%Y6/Y6+10%PCE10-2F	0.784	25.98	69.97	14.30
PCE10-2F+20%Y6/Y6+20%PCE10-2F	0.783	25.64	69.30	13.94
PCE10-2F+40%Y6/Y6+40%PCE10-2F	0.781	25.34	67.72	13.43

Table S5. The detailed data of hole and electron mobility, the exciton generation rate (G), and the exciton dissociation efficiency (η_{diss}).

Device	μ_h ($10^{-4}\ cm^2\ V^{-1}\ s^{-1}$)	μ_e ($10^{-4}\ cm^2\ V^{-1}\ s^{-1}$)	μ_h/μ_e	G ($nm^{-3}\ s^{-1}$)	η_{diss} (%)
PCE10-2F/Y6	4.27	3.26	1.31	18.52	96.95
M-PCE10-2F/Y6	4.45	3.71	1.20	19.76	97.35
PCE10-2F/M-Y6	4.68	4.04	1.16	19.91	97.54
M-PCE10-2F/M-Y6	4.91	4.66	1.05	22.48	97.86

Table S6. Detailed energy loss of optimal devices.

Device	E_g (eV)	ΔE_1 (eV)	ΔE_2 (eV)	ΔE_3 (eV)	E_{loss} (eV)	EQE_{EL} (%)
PCE10-2F/Y6	1.376	0.264	0.054	0.272	0.590	2.53×10^{-3}
M-PCE10-2F/Y6	1.372	0.264	0.057	0.266	0.587	3.19×10^{-3}
PCE10-2F/M-Y6	1.364	0.264	0.056	0.259	0.579	4.19×10^{-3}
M-PCE10-2F/M-Y6	1.362	0.264	0.057	0.254	0.575	5.09×10^{-3}

Table S7. Summarized photovoltaic parameters of PCE10-2F/Y6 and M-PCE10-2F/M-Y6 semitransparent organic solar cells at 15 nm and 25 nm Ag conditions.

Active layer	Electrode (nm Ag)	*V*oc (V)	*J*sc (mA/cm^2)	FF (%)	PCE (%)	AVT (%)	LUE (%)
PCE10-2F/Y6	15	0.777	19.46	68.89	10.48	44.46	4.66
	25	0.778	19.78	69.56	10.72	40.53	4.34
M-PCE10-2F/M-Y6	15	0.782	20.36	70.93	11.32	43.25	4.90
	25	0.783	20.61	71.20	11.50	39.36	4.53